T.C.L.G. SOLLNER, E.R. BROWN, and H.Q. LE

Microwave and Millimeter-Wave Resonant-Tunneling Devices

Resonant-tunneling devices, which may be capable of operation at terahertz frequencies, have been developed and tested. Included in these solid state microelectronic components are oscillators, self-oscillating mixers, and harmonic multipliers. A characteristic of these devices, negative differential resistance (NDR), has been observed at room temperature. Resonant-tunneling transistors, which promise operation in the terahertz frequency range, are also proposed.

PHYSICS OF RESONANT TUNNELING

A resonant-tunneling diode can respond to electrical impulses in picosecond or subpicosecond times. Therefore, these devices may provide a basis for developing electronic devices that operate at terahertz frequencies.

The essential features of resonant tunneling are shown in Fig 1. A thin layer of GaAs (2 to 10 nm) is sandwiched between two thin layers of $Al_xGa_{1-x}As$. The addition of aluminum to GaAs raises the band-gap above that of GaAs so the $Al_xGa_{1-x}As$ regions act as partially transparent mirrors to electrons; the higher energy level of these barriers reflects the electrons back to the region of the structure from which they came. The charge transport across the structure takes place by tunneling through the thin (1 to 5 nm) $Al_xGa_{1-x}As$ barriers.

This structure is the electron analog of a Fabry-Perot resonator. As shown schematically at the bottom of Fig. 1, the resonator exhibits peaks in the electron transmission (current) as the incident electron energy (voltage) changes.

The physical implementation of these principles is summarized in Fig. 2. The layered material is grown in wafer form by molecular beam epitaxy. Then the active regions are defined with ohmic contacts. These contacts are used as a mask to isolate the region under the contact, either by etching mesas (as shown in Fig. 2), or by proton implantation, which makes the surrounding material nonconductive. Because the contact is only a few microns in diameter, electrical connection to the ohmic contact is made with a pointed wire (whisker). In some cases, the whisker acts as an antenna, coupling high-frequency ac fields to the double-barrier diode.

Using the Fabry-Perot analogy, coherence of the electron-wave function is required across the entire double-barrier region to maintain resonant tunneling. Any scattering that occurs in either the well or the barriers will alter the wave function phase randomly, destroying its coherence and therefore, the conditions required for resonant tunneling. But a different picture (see Appendix, "Resonant Tunneling Theory"), one that does not require coherence between the parts of the wave function outside and inside the well, can produce negative resistance, the essential characteristic that is exploited in the devices that are described in this article.

In 1973, Tsu and Esaki [1] derived the two-terminal current-voltage (I-V) curves for finite multiple-barrier structures. This matching technique has been remarkably successful in explaining experimental results. In 1974, Chang *et al* [2] were the first to observe resonant tunneling in a monocrystalline semiconductor. They used a two-barrier structure and observed the resonances in the current by measuring the I-V curve of the structure. The voltages at the current peaks agreed well with Chang's calculations.

A decade later, interest in the field was renewed when Sollner *et al* [3] showed that the intrinsic charge transport mechanism of a two-barrier diode could respond to voltage changes in less than 0.1 ps (> 1 THz). More recently, negative differential resistance (NDR), a characteristic of resonant tunneling, has been measured at room temperature [4].

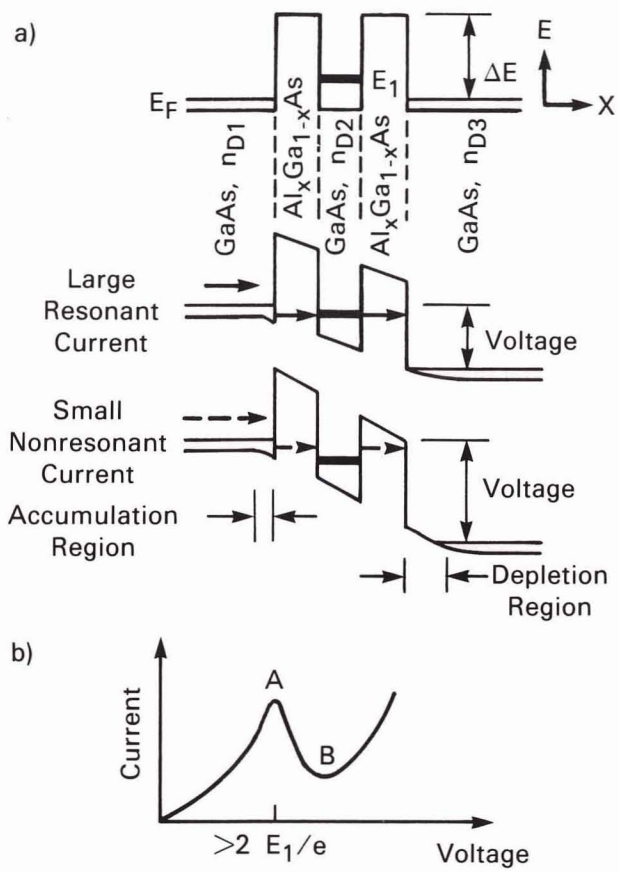

Fig. 1(a) — The energy profile of an electron in a double-barrier resonant-tunneling structure is shown here. The top illustration, which includes the energy well produced by the two $Al_xGa_{1-x}As$ layers, shows the unbiased energy profile. The $Al_xGa_{1-x}As$ layers act as partially transparent mirrors to the electrons, similar to a Fabry-Perot resonator. (b) In this plot of diode current as a function of incident electron energy, the large resonant current at point A corresponds to the energy profile of A; the valley in the current-profile at point B corresponds to energy profile of B. Although the energy of incident electrons is higher at B, the absence of resonance lowers the current.

SPEED OF RESPONSE

Two factors indicate that the response time of a double-barrier resonant-tunneling structure should be as little as 0.1 ps: the resonant-state lifetime of an electron and the time required for a double-barrier structure to reach equilibrium after an electrical impulse. This predicted response time is the time required for the device's current to respond to a sudden change in voltage. The comparison of the measured and predicted times not only gives an indication of the accuracy of the models, it also indicates the fundamental limits of operation imposed by the structure of double-barrier devices. One of the most significant limits of operation is f_{max}, the maximum useful frequency at which the device exhibits NDR. This frequency is the point above which NDR is no longer observable at the terminals of the device.

If the voltage across a double-barrier structure is instantaneously changed, the current through the device changes to a different steady-state value. As in a Fabry-Perot resonator, the steady-state charge in the well must decrease when the current decreases, and increase when the current increases. The lifetime of any resonant state, including the one represented by an electron initially placed in the well between the two barriers of a resonant-tunneling structure, is given by $\tau = \hbar/\Delta E$, where ΔE is the energy half-width of the transmission probability function through the resonant state. It takes approximately one lifetime to fill or empty the well to a new steady-state value. Since the carrier transmission probability is determined by the amplitude of the wave function inside the well, the current will reach its new steady-state value in approximately the lifetime of a resonant state.

The lifetime of an electron in between the barriers has been calculated for three representative structures by Sollner *et al* [5] and ranges from 4 ps for a 2.5-nm AlAs barrier to 0.16 ps for a 3.0-nm $Ga_{0.7}Al_{0.3}As$ barrier. In Table 1, this time is found from $\tau = 1/(2\pi f_{\Delta E})$. The transit of electrons across the structure's depletion region produces an additional delay that ranges from 0.16 to 0.69 ps. Total delays, the *intrinsic* response times, therefore range from 0.4 to 5.0 ps.

For signals with periods much shorter than the intrinsic response time, the current lags the applied voltage and the I-V curve for the high-speed signals should deviate markedly from the dc I-V curve. The intrinsic response time was first measured experimentally by examining the difference between the dc I-V curve measured and the I-V curve inferred from high-frequency measurements. Because the response times were in the picosecond range,

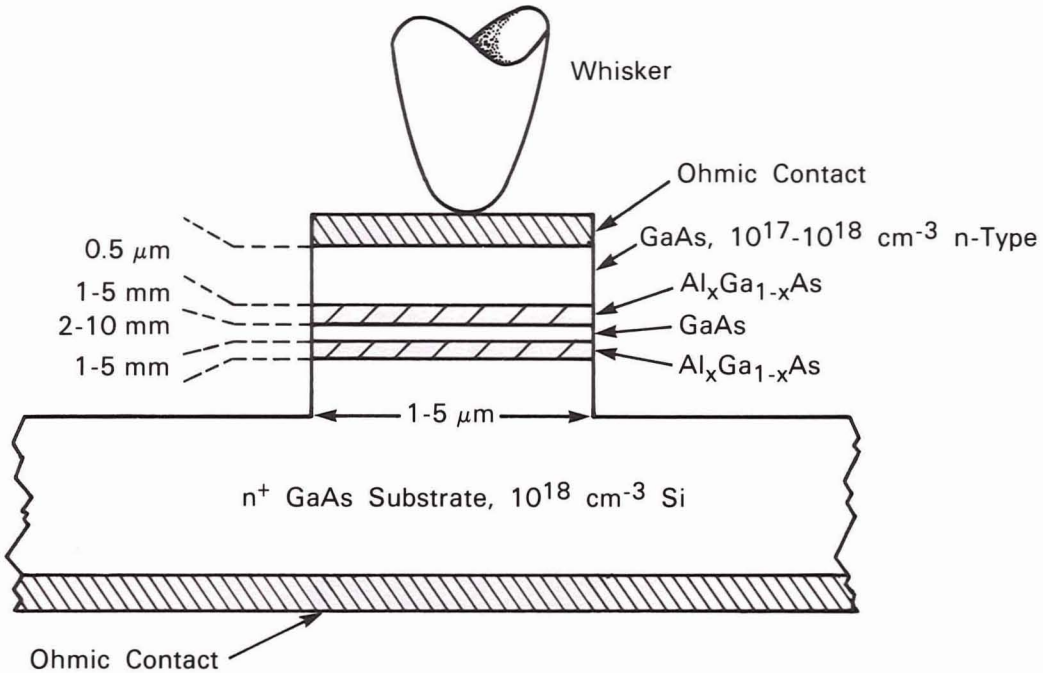

Fig. 2 — This double-barrier diode has 1- to 5-nm barriers and a 2- to 10-nm well.

operation at terahertz frequencies was necessary.

The straightforward approach to determining the frequency response of a device is to sweep through the I-V curve at increasing speed until the measured I-V curve differs from the dc curve. Unfortunately, it is difficult to measure current at frequencies above those accessible to sampling oscilloscopes (100 GHz). Therefore, we used a differential measurement technique. We swept through a large, low-frequency voltage-range and measured the diode current with relatively simple conventional techniques. At the same time we superposed a small high-frequency signal across the diode. The low-frequency current revealed changes in curvature of the I-V curve that were proportional to the high-frequency signal. Besides tractability, this method of measurement closely resembles the actual operating conditions of devices which utilize NDR. In practical operation, a device is biased into the negative differential region by a large dc bias and the superposed voltage doesn't extend far outside the NDR region.

The circuit used for applying ac and dc fields to the double-barrier diode is shown in Fig. 3. The corner-reflector mount was originally developed for Schottky-diode mixers in the far infrared [6]. Frequencies between dc and about 20 GHz can be applied through the coaxial connector via the whisker that contacts the active area. The GaAs substrate is soldered to the chip stud, which is at the same ground potential as the corner reflector. For frequencies of about 100 GHz to a few terahertz, the long whisker acts as an antenna, and the conducting surfaces cause images of the whisker to produce an antenna array. The array will receive energy in a beam that has a frequency-dependent direction, but is approximately 45° from all surfaces of the cube. The full cone-angle of the beam is about 20°.

For the 2.5-THz measurements, for example, the power produced by an optically pumped methanol laser (about 100 mW) was matched to the antenna pattern with a lens, thus coupling about 50% of the incident power onto the antenna and producing an ac signal across the double-barrier structure. The characterization of the corner-reflector mount at lower frequencies (using measurements performed by Fet-

terman *et al*) led to an estimate of 50 Ω for the antenna impedance Z_A. This parameter was used in Eq. (1) to calculate the curves in Fig. 4.

At high frequencies the current responsivity R_i, which is the change in dc current (ΔI), divided by the change in ac power applied, (ΔP_{ac}), is given by

$$R_i(V) = \frac{\Delta I(V)}{\Delta P_{ac}} = \frac{2I''(V)Z_A}{(1+Z_A/R_s)^2}\left(\frac{1}{\omega R_s C}\right)^2 \qquad (1)$$

In Eq. 1, I″ is the second derivative of the I-V curve at the ac frequency of interest. This expression gives the I-V curve for current responsivity measured over the voltage range of interest. Measurements were made at 1, 138, 761, and 2,500 GHz on a double-barrier diode with 3.0-nm well and barriers. The results at dc, 1 GHz and 2.5 THz are shown in Fig. 4. The measurements for 138 and 761 GHz were essentially identical to the 1-GHz curve. Since the 1-GHz signal's period is long compared with the expected intrinsic response time, deviation in the I-V curve shouldn't occur until frequencies that are orders of magnitude higher are reached. The reason for the change between dc and 1 GHz is not known, but it is probably due to slow traps in the material.

By 2.5 THz, the diode's I-V curve looks quite different from the dc curve. In one direction, NDR has vanished, but it remains in the other direction. Sollner *et al* [3] take this as evidence that the intrinsic response time for this device is of the order of $\tau = (2\pi f)^{-1} = 6 \times 10^{-14}$ s. This result agrees approximately with theoretical

Table 1 — Measured and Calculated Parameters for Three Different Wafers of Double-Barrier Diodes

	Wafer		
	1	*2*	*3*
Material Parameters			
Barrier material	AlAs	$Ga_{0.7}Al_{0.3}As$	AlAs
Barrier thickness (nm)	2.5	3.0	1.5
Well thickness (nm)	4.5	4.5	4.5
Doping outside barriers (cm^{-3})	1×10^{18}	2×10^{17}	2×10^{17}
Electrical Parameters			
Peak-to-valley ratio, 300 K	1.7/1	1.3/1	3.5/1
Peak current density ($\times 10^4$ A cm^{-2})	0.8	1.2	4.0
Depletion layer at bias (nm)	15	30	70
Capacitance (fF)[a]	100	50	20
Maximum negative conductance (mS)[a]	5.0	8.0	13.0
Series resistance (Ω)[a]	10	15	15
Oscillation Characteristics			
DC bias I_B, V_B (mA, V)	0.7, 0.40	2.7, 0.32	3.0, 0.95
f_{osc} (GHz)[b]	20.7	43.7	201
Theoretical			
Maximum Oscillation Frequency			
f_{max} (GHz)[c]	35	70	270
f_{depl} (GHz)[d]	1,000	500	230
$f_{\Delta E}$ (GHz)[e]	40	1,000	400

[a]Typical values for a circular mesa of 4-μm diameter.
[b]Maximum observed fundamental oscillation frequency.
[c]$f_{max} = (2\pi C)^{-1}(-G_{max}/R_s - G_{max}^2)^{1/2}$
[d]From depletion layer drift time assuming a drift velocity of 10^7 cm/s.
[e]From calculation of energy width of transmission through double-barrier structure.

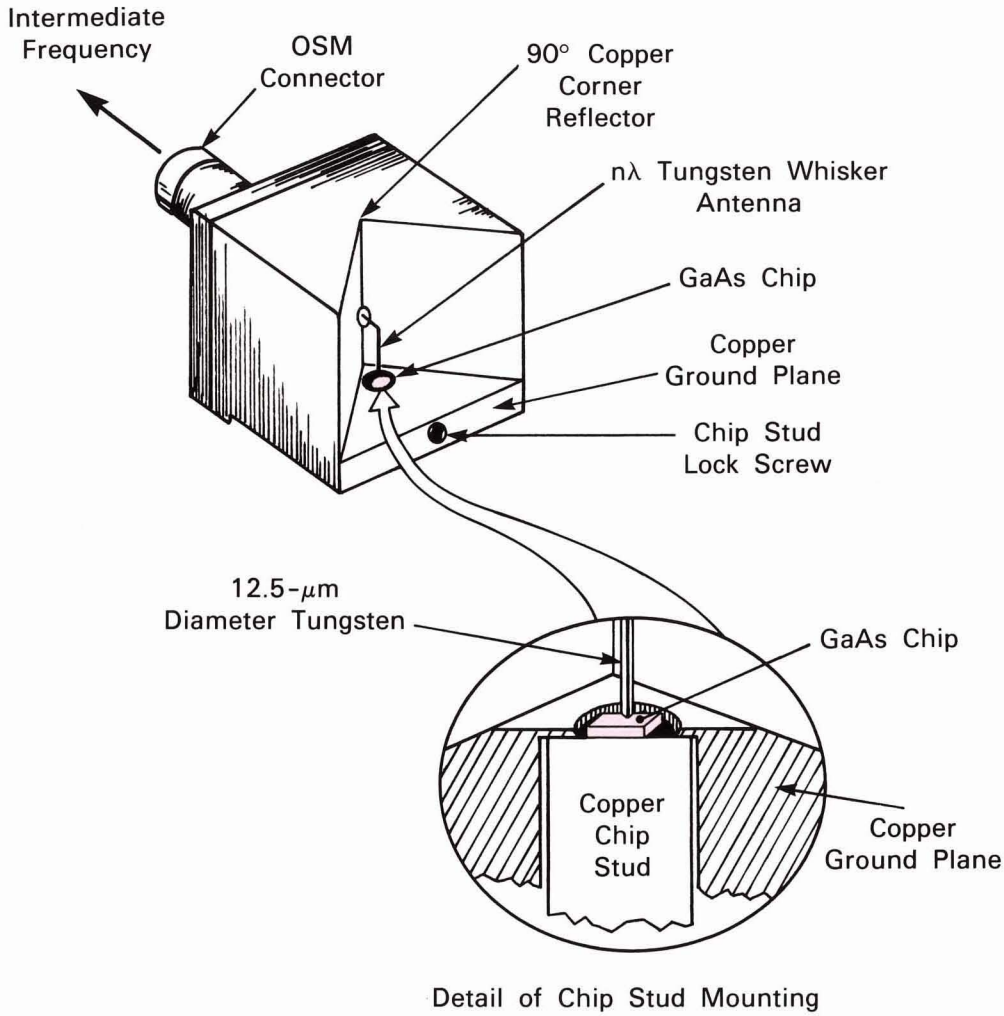

Fig. 3 — This corner-reflector mount is used to apply signals to double-barrier diodes. For frequencies between dc and 20 GHz, the signal is coupled through the OSM connector. Above 100 GHz, the long whisker acts as an antenna, coupling the signals into the chip from a full cone-angle of about 20°.

expectations from Table 1 for 3-nm barriers of $Al_{0.25}Ga_{0.75}As$ ($f_{\Delta E} = 1 \times 10^{15}$). The asymmetry of both the dc I-V curve and the response may indicate that the two barriers or the two depletion regions are not identical.

The double-barrier diode's equivalent circuit, shown in Fig. 5, provides a model for further understanding of this device. Included in the equivalent circuit are the voltage-dependent dynamic conductance G(V), the series resistance R_s, and the parallel capacitor C that is inherent in the device structure. To a good approximation, the capacitance is formed across a combination of the two barriers plus the depletion region on the anode side of the biased device. The slope of the low-frequency I-V curve gives the approximate conductance, *ie*, $(dI/dV)^{-1} = R_s + 1/G \approx 1/G$.

RESONANT-TUNNELING OSCILLATORS

The NDR displayed by the double-barrier diode is the basis of a fast and simple two-terminal oscillator. Interest in the oscillator application stems from the need for a solid state oscillation source at frequencies above 300 GHz. In this region, few fundamental-mode solid state sources are available, so the double-barrier diode would be useful for applications

that require only modest amounts of power. Furthermore, these oscillations give a direct and unmistakable proof of the speed of these devices. Of course, inherent circuit elements, particularly the series resistance and the device capacitance shown in Fig. 5, must be considered for circuit applications of these devices.

In the further analysis required for circuit applications, the conductance, $G(V_0)$, is independent of frequency but strongly dependent on the voltage amplitude, V_0, across the device. The real part of the impedance, Z_D, measured across the equivalent circuit of Fig. 5 is negative up to a frequency given by the expression

$$f_{max} = \frac{1}{2\pi C}\left(\frac{-G_{max}}{R_s} - G_{max}^2\right)^{1/2} \qquad (2)$$

where G_{max} is the maximum negative value of dynamic conductance in the NDR region of the I-V curve. For all frequencies above f_{max}, the real part of the terminal impedance will be positive, making it impossible for oscillations to occur.

Brown *et al* [7] found double-barrier diode oscillators that cover the frequency range of 20 to 200 GHz (frequencies below f_{max}). Figure 6 shows the experimental results obtained in this range with diodes from the wafers listed in Table 1. The initial experiments were performed with a device from Wafer 1 in a coaxial resonator, giving an oscillation frequency of 20.7 GHz and an output power well below 1 W. Attempts to achieve oscillation with this device at frequencies near 40 GHz in a WR-22 waveguide resonator were unsuccessful, consistent with the theoretical f_{max} of 35 GHz. The first millimeter-band results were obtained in the vicinity of 30 GHz and 40 GHz in WR-22 and WR-15 waveguide resonators, respectively, using a device from Wafer 2. This device could have achieved higher oscillation frequencies, but because of the relatively low peak-to-valley ratios of devices from Wafer 2, no attempt at higher oscillation frequencies was made. The wafer's low peak-to-valley ratio indicates that devices from this wafer will provide limited power output and logic-swing capability.

The voltage range over which NDR exists for these devices limits the output power of oscillators that use them. Kim and Brandli [8] and

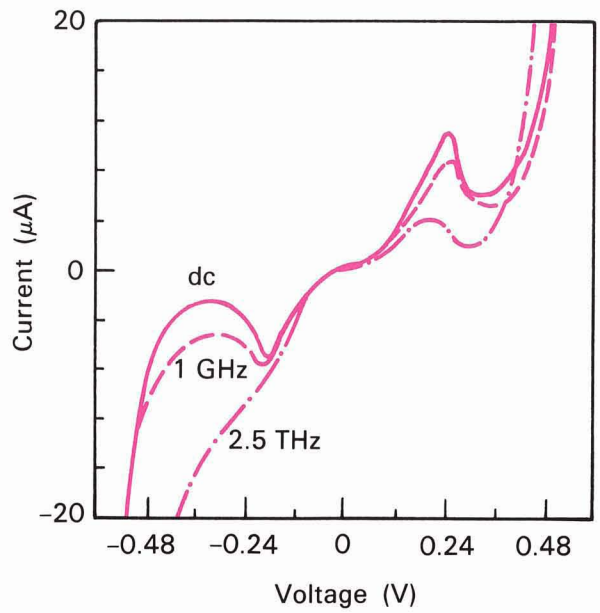

Fig. 4 — The current-voltage (I-V) curves of a double-barrier diode show the variation with frequency of the device's negative differential resistance — it essentially disappears at 2.5 THz.

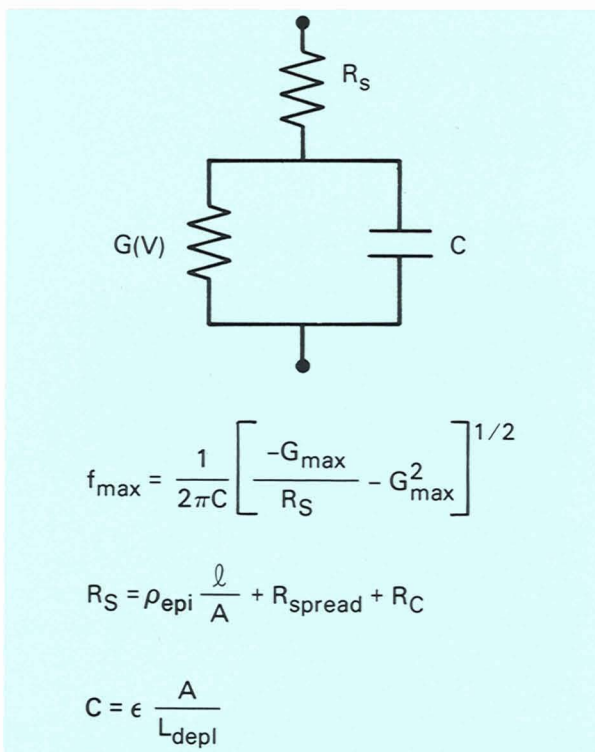

Fig. 5 — Using this equivalent circuit, the double-barrier diode's maximum frequency of oscillation can be easily calculated.

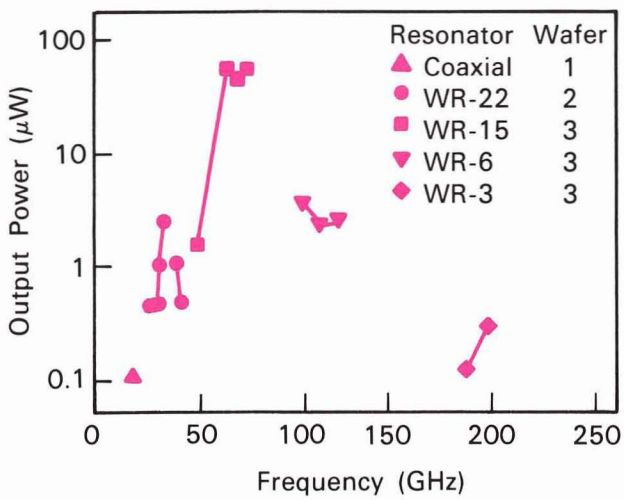

Fig. 6 — The output power versus frequency of resonant-tunneling diodes for three different wafers was measured in five different resonators.

Trambarulo [9] have shown that the maximum output power, assuming a sinusoidal voltage waveform, is $P_{max} = (3/16)\Delta I/\Delta V$, where ΔI and ΔV are the current and voltage ranges of the negative resistance region. For the 4-μm-diameter diodes of Wafer 3 in Table 1, this relation gives $P_{max} \approx 225\ \mu W$. Diodes of larger area can produce more output power, but G_{max} scales linearly with diode area, making it very difficult to obtain dc stability in larger devices. All of the 4-μm-diameter devices tested to date have been stabilized with standard 50 Ω coaxial loads.

Diodes from Wafer 3 have produced the most powerful oscillations and the highest oscillation frequency to date. This wafer extended the maximum observed oscillation frequency of resonant-tunneling diodes from 56 to 201 GHz. The output power produced at 201 GHz was about 0.2 μW, although it reached 60 μW at lower frequencies. Several of the diodes tested did not oscillate at all. The difficulty in initiating oscillations near 200 GHz is consistent with Eq. 2, which predicts that $f_{max} \approx 270$ GHz for this diode.

The Fig. 5 model is identical to that used for p-n junction tunnel diodes. Indeed, the double-barrier resonant-tunneling diode and the p-n junction tunnel diode are similar, displaying similarities in I-V characteristics and in circuit behavior. The major difference between the two types of diodes is in the magnitude of their parasitics. In the p-n junction tunnel diode, very high doping densities are required on both sides of the junction ($N \leqslant 1 \times 10^{19}$ cm^{-3}) to achieve a high tunneling current density. This high doping density creates a short depletion layer and therefore a relatively large specific capacitance. The double-barrier diode, however, can achieve a high current density with much lower doping densities on both sides of the structure ($N \approx 10^{17}$ to 10^{18} cm^{-3}).

A good figure of merit for comparing the speed of different diodes is the ratio of specific capacitance to peak current density, $\gamma = C_S/J_P$. This ratio is known as the speed index [10]; it is a measure of the current available for charging the device capacitance. For Wafer 3, this quantity is $\gamma \approx 1 \times 10^5$ pF cm^{-2}/4.0×10^4 A cm^{-2} = 3.0 ps/V. The fastest p-n junction tunnel diodes ever reported [11] were made of GaAs and had γ = 14 to 16 ps/V, nearly a factor of five poorer than the double-barrier devices. Moreover, the p-n junction tunnel diodes [12] achieved a maximum experimental oscillation frequency of only 103 GHz with an output power well below 1 μW.

SELF-OSCILLATING MIXERS

Near the NDR region in an I-V curve, a resonant-tunneling diode's dynamic conductance varies rapidly as a function of the applied signal voltage. This feature makes the resonant tunneling diode an efficient mixer. The Fourier series of the diode's dynamic conductance has large components at the oscillation frequency f_0 and its first few harmonics, particularly the even harmonics when the I-V curve is antisymmetric about the bias point. The relative strength of these components will determine the efficiency of power conversion from the signal frequency f_S to the intermediate frequency f_I, assuming that $f_S > f_I$. In the fundamental mode of conversion, the signal has frequency $f_S = f_0 \pm f_I$, and in the second-harmonic mode, the signal frequency is $f_S = 2f_0 \pm f_I$. The most efficient conversion should be in the second-harmonic mode at the dc bias point of maximum negative resistance, because this

point has approximate antisymmetry in the I-V curve [*ie*, I(V) = -I(-V)]. However, the fundamental mode should achieve its maximum efficiency at bias voltages nearest the regions of greatest curvature, where the Fourier series of g(t) has a predominant coefficient at the oscillation frequency.

The resonant-tunneling self-oscillating mixer has the potential to displace the Schottky diode in many millimeter-wave applications. To do this, it must demonstrate a competitive noise figure, roughly 3 to 6 dB in the microwave region and 6 to 10 dB in the millimeter band. Although noise figures have not yet been studied, measurements of stable resonant-tunneling diodes indicate that they have very low intrinsic noise [13]. In fact, the measured noise power is less than expected from the full shot noise expression, for reasons that are not fully understood. Nevertheless, this low noise figure will undoubtedly work to the benefit of the resonant-tunneling-diode-based self-oscillating mixer. And the resonant-tunneling self-oscillating mixer provides the intrinsic capability to achieve conversion gain. Mixers such as the standard Schottky diode aren't capable of gain and usually show losses of several decibels.

Using the fundamental mode of coaxial resonant tunneling oscillators, we have operated them as mixers in the microwave region. Shown in Fig. 7 is the mixing spectrum of an oscillator with an oscillation frequency of 14.2 GHz, a signal frequency of 8.2 GHz, and an intermediate frequency of 6.0 GHz. The single-sideband conversion loss in this case is just under 6 dB,

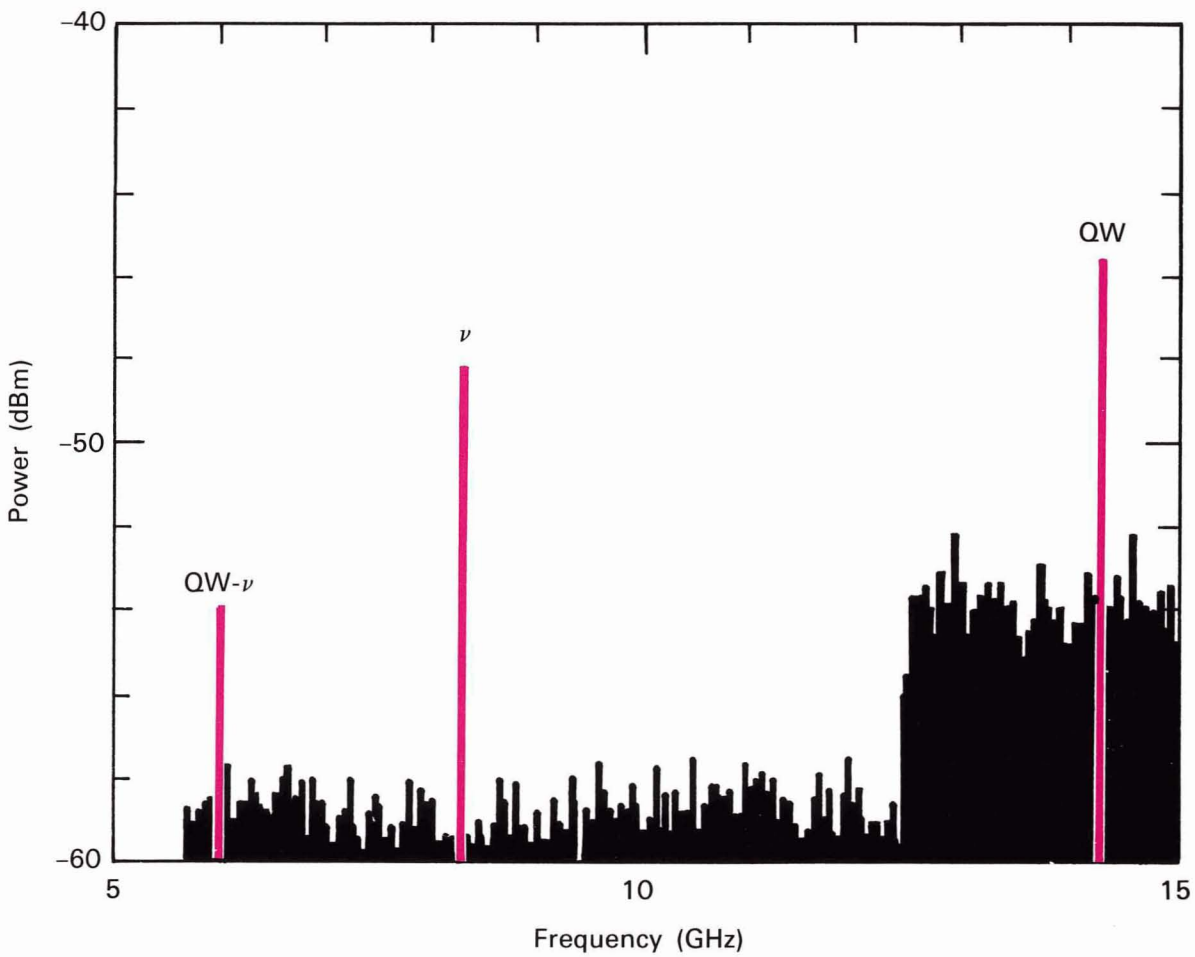

Fig. 7 — The frequency down-conversion of a signal at frequency ν by a double-barrier diode oscillating at the frequency marked QW produces the difference frequency labeled QW-ν.

which is only about 3 dB higher than the best results for room-temperature Schottky-diode mixers in the same frequency region. The experiments on the second-harmonic mode have just begun, using a waveguide oscillator in the millimeter band. The best conversion loss achieved to date is about 12 dB for an oscillation frequency of 50 GHz and a signal frequency of 100 GHz. This performance is comparable to the best results reported for a pair of Schottky diodes in the antiparallel configuration [14].

RESISTIVE MULTIPLIERS

Resonant-tunneling devices excel as resistive multipliers. A resistive multiplier, which is a form of harmonic multiplier, generates power at frequencies that aren't conveniently available from fundamental oscillators. Harmonic multipliers are often used for radio astronomy. In radio astronomy, heterodyne receivers, operating at frequencies above 100 GHz, use power from a harmonic multiplier as a local oscillator source. Harmonic multipliers are also the primary source of power for molecular spectroscopy in the submillimeter wavelength spectrum.

Currently, resistive multipliers usually use Schottky-barrier diodes, but the advantages of resonant-tunneling diodes will promote their use as resistive multipliers. The absence of even harmonics in a resonant-tunneling diode's dynamic conductance simplifies the design of multiplier circuits, particularly in the millimeter-wave region. Also, because of its negative resistance, the maximum theoretical generation efficiency of a double-barrier diode can be significantly higher than an ideal diode's n^{-2} (where n is the harmonic number) [15].

If a resonant-tunneling diode is pumped so that the peak amplitude of the voltage across the diode occurs above the device's resonant-current peak, at least three local maxima in the diode's current waveform will be produced over one cycle. (See Fig. 8 for a theoretical curve.) These maxima correspond to third- or higher-order odd-harmonic generation. The ease with which these higher-order odd harmonics are obtained is due to the presence of a peak and a valley in the diode's I-V curve, as well as the

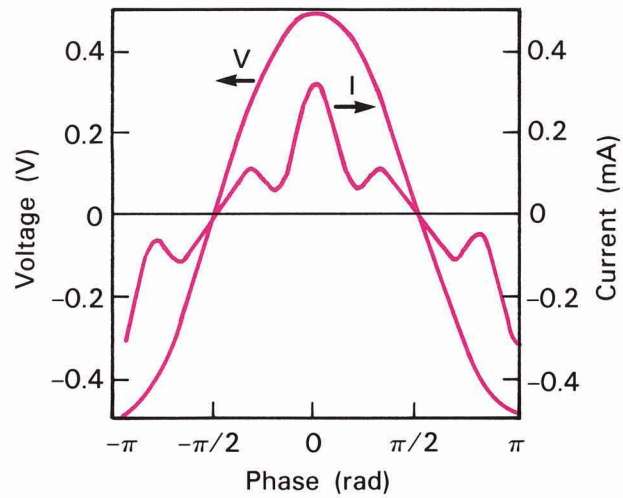

Fig. 8 — Voltage and current waveforms for a double-barrier diode reveal that the local maxima in the current waveform, if equally spaced in phase, should lead to a strong fifth harmonic component in the current-power spectrum.

overall antisymmetry of this curve about the origin.

To demonstrate this odd-harmonic generation, a diode's I-V curve can be modeled with a seventh-order polynomial. Using this model, the diode is assumed to be driven by a source that has an internal impedance less than the minimum negative resistance of the double-barrier diode. Thus the current across the diode is a single-valued function of the drive voltage. The numerically determined current-waveform of an 0.5 V source is shown in Fig. 8. The local maxima in this waveform, if equally spaced in phase, should lead to a strong fifth harmonic component in the current-power spectrum. This spectrum, shown in Fig. 9, predicts that the available fifth-harmonic power will be 0.065 times that of the fundamental.

Figure 10 illustrates the power spectrum obtained for a resonant-tunneling diode that was mounted in a 50 Ω coaxial circuit and pumped at 4 GHz. As expected, even harmonics are absent and the fifth harmonic predominates among the odd harmonics. However, the measured efficiency was only about 0.5%, significantly less than the theoretical prediction of 6.5%. This discrepancy can possibly be attributed to the test circuit, which does not allow

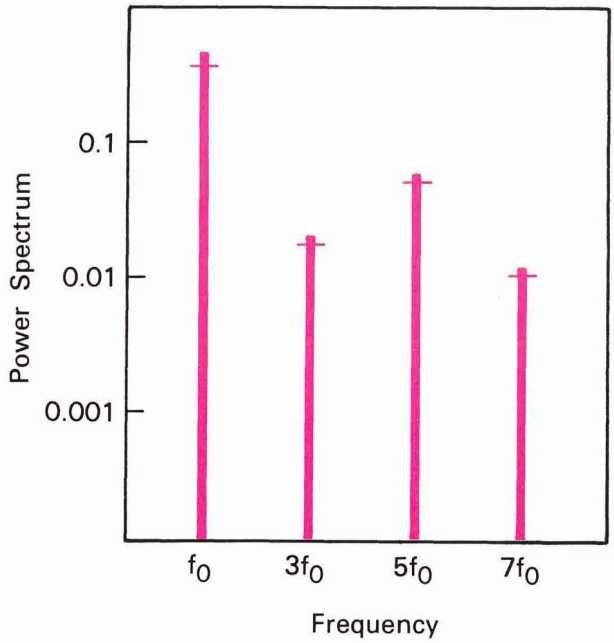

Fig. 9 — A power spectrum corresponding to the voltage-current plot of the Fig. 8.

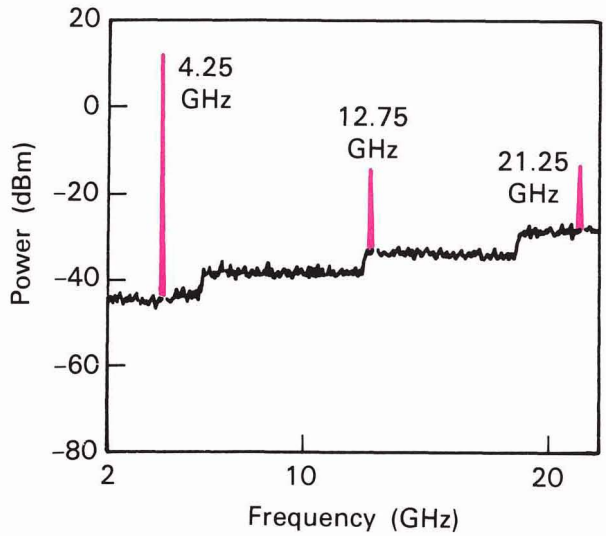

Fig. 10 — A strong fifth-harmonic component was confirmed experimentally for a 4.25-GHz input signal.

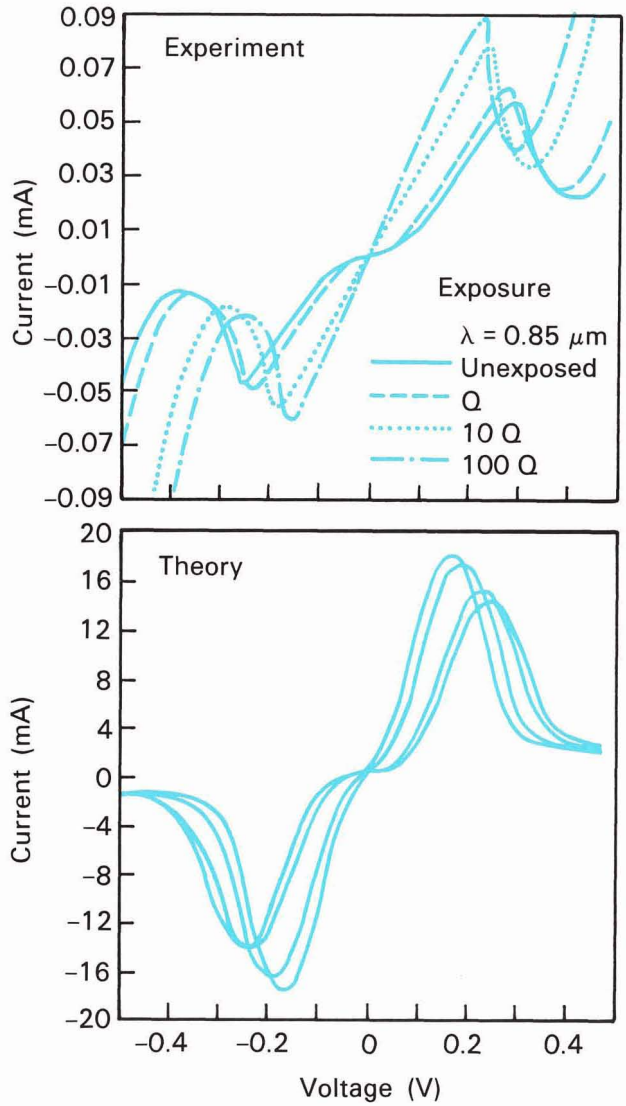

Fig. 11 — Persistent photoconductivity is a characteristic of resonant-tunneling diodes. The experimental results were obtained from a diode that was cooled to 20 K in the dark and then exposed to progressively greater levels of light.

independent tuning of the harmonics. Ideally, the fifth harmonic should be terminated with a resistance greater than the source resistance. But the third harmonic should be terminated with a reactance, which eliminates power dissipation and reinforces the fifth-harmonic voltage. Combining these features in a one circuit will allow independent tuning of the harmonics and greater conversion efficiency for the fifth harmonic.

PERSISTENT PHOTOCONDUCTIVITY AND A RESONANT-TUNNELING TRANSISTOR

A transistor based on a double-barrier resonant-tunneling structure could significantly improve upon the present state of the art. Persistent photoconductivity provides clues to the operation of such a transistor, wherein the well region acts as the device's control electrode.

A resonant-tunneling structure sometimes exhibits persistent photoconductivity [16], that is, the structure's I-V curve shifts with successive exposures to light. Figure 11 illustrates this shift. Photoionization of DX centers in the $Al_{0.3}Ga_{0.7}$ barriers in the structure causes the shift in the I-V curve. (DX centers are lattice vacancies associated with a nearby donor atom. For a detailed discussion of DX centers, see Nelson [17] or Lang *et al* [18].) This photoionization creates a dipole region with fixed positive charge in the barriers and free electrons outside the barriers. Any electrons that reside initially in the well quickly escape because of the higher energy of the confined band edge within the well and the short resonant-state lifetime. The dipoles produce the band bending shown in Fig. 12. The well is lowered in potential by an amount $\Delta\phi$, and the barriers are also lowered. The resulting shifted I-V curve shows a peak transmission that has been moved to a lower voltage by the lowered well and a higher current density caused by the lower effective barriers.

Figure 12 shows that DX centers in the barriers provide a way of adjusting the well potential relative to the outer contact regions. This effect is analogous to the modulation of the base potential of a conventional transistor. In this case, the structure's potential well serves as the control electrode.

The transconductance of such a device, G_m, is related to the change in collector current density, ΔJ_c, and the change in well potential, $\Delta\phi$, by

$$G_m \equiv \frac{\partial I_c}{\partial V_{be}} = \frac{A\Delta J_c}{\Delta\phi} \tag{3}$$

where A is the emitter area. The shift in the well potential is approximately related to the shift in the current peak ΔV_p by

$$\Delta V_p \approx 4\Delta\phi \tag{4}$$

This expression is valid only for the specific diode of Sollner *et al* [19]. One factor of two on the right side approximately accounts for the depletion region on the collector side when biased to the current peak. The other factor of two arises from the base-to-emitter voltage,

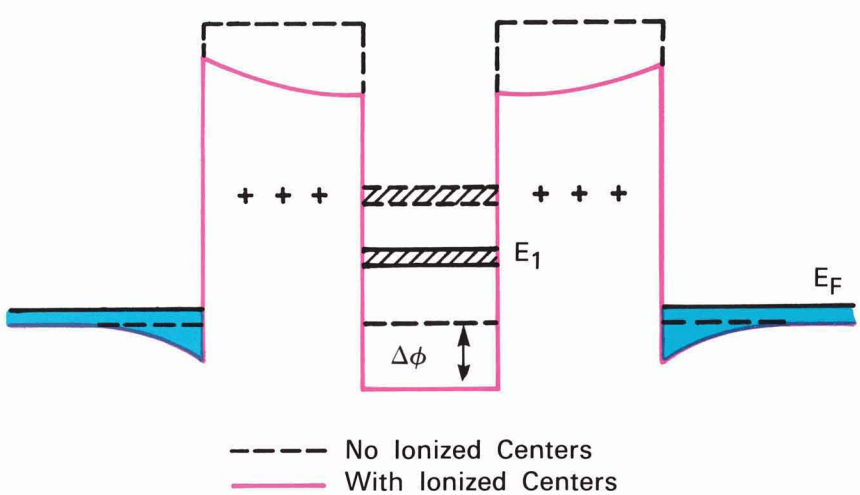

Fig. 12 — Positive charge in the barriers of a double-barrier diode produces band bending (red line); a device without ionized centers has no band bending (black line).

which is, at most, half of that applied between the base and collector. Thus the transconductance becomes

$$G_m = \frac{4A\Delta J_c}{\Delta V_p} \tag{5}$$

But there is one complication. The leakage current also changes with $\Delta\phi$, but this change is probably related to the presence of DX centers in the barriers rather than to the modulation of the well potential. To account for this contribution, we assume that, at voltages below the current peak, the transistor output impedance is large and positive, so we can extrapolate the excess current at high voltage back to zero and keep the output impedance positive. These extrapolations are shown in Fig. 13. Using this figure, an emitter width of 1 μm gives an intrinsic transconductance of 4,000 mS/mm. Specific contact resistances of the order of $10^{-7}\ \Omega\ cm^2$ are necessary to realize such a high extrinsic transconductance.

The frequency above which the small-signal short-circuit current gain drops below unity is

$$f_T = \frac{C}{2\pi G_m} \tag{6}$$

where C is the total input capacitance. Using a 1-μm gate contact and 40-nm n^- regions, we find f_T = 110 GHz.

The maximum frequency of oscillation f_{max} will also depend on the base resistance. For negligible emitter resistance,

$$f_{max} = \frac{f_T}{4R_bC_c} \tag{7}$$

where Rb is the base resistance and C_c is the base-to-collector capacitance. As the base is very thin and lightly doped, it might be expected

Symbols

Units are shown in brackets.

A	Cross-sectional area of a device [cm^2]
C	Capacitance [F]
C_c	Collector capacitance [F]
C_S	Capacitance per unit area [F/cm^2]
E_f	Fermi energy [J]
e	Charge on the electron [C]
f_I	Intermediate frequency [Hz]
f_{max}	Frequency above which the terminal conductance is positive for all voltages, hence maximum oscillation frequency [Hz]
f_O	Output frequency [Hz]
f_S	Signal frequency [Hz]
f_T	Frequency above which the small-signal short-circuit current gain is below unity [Hz]
$f_{\Delta E}$	Frequency corresponding to resonant-state lifetime [Hz]
G_{max}	Maximum negative value of voltage-dependent conductance [S]
G(V)	Voltage-dependent conductance of a resonant-tunneling diode [S]
g(t)	Conductance of a diode modulated by a changing voltage [S]
I	Current [A]
IF	Intermediate frequency [Hz]
J_c	Collector current density [A/cm^2]
J_P	Peak current density [A/cm^2]
n_0	Carrier concentration [cm^{-3}]
P_{max}	Maximum output power obainable from a negative-resistance amplifier [W]
R_b	Base resistance [Ω]
R_i	Current responsivity [A/W]
R_s	Series resistance [Ω]
V	Voltage [V]
V_0	Voltage amplitude [V]
v_m	Voltage at frequency m [V]
Z_A	Antenna impedance [Ω]
Z_D	Device impedance [Ω]
Z_L	Load impedance [Ω]
ΔE	Energy half-width of transmission function [J]
ΔI	Current excursion of negative differential resistance region [A]
ΔE	Change of current [A]
ΔP_{ac}	Change of ac power [W]
ΔV_p	Shift of the voltage of the current peak from ionized charges in the barriers [V]
ΔV	Voltage excursion of negative differential resistance region [A]
$\Delta\phi$	Shift in potential of the well from ionized charges in the barriers [eV]
ϵ	Dielectric constant [F/cm]
γ	Speed index [s/V]
ω	Angular frequency [s^{-1}]
$\phi(x)$	Electrostatic potential energy [eV]

that the base resistance would be high. However, the quantum-well geometry reduces the resistance considerably. Electron mobilities in modulation-doped quantum wells are very high at temperatures less than 100 K. Although this structure is not a modulation-doped well in the usual sense, the base layer near the resonant current peak acquires charge from the transiting carriers without any direct doping [20]. For present samples, the average well-charge density is approximately 10^{17} cm^{-3}.

Using a mobility of 5×10^5 $cm^2/V\text{-}s$ for a base carrier density 2×10^{17} cm^{-3} (the best mobility [21] at 50 K), a 1×20-μm emitter, and a 4.0-nm well thickness, the base resistance is less than 10 Ω. This gives an R_bC_c product of about 0.5 ps, resulting in an f_{max} of 330 GHz. Any increase in current density increases f_T and f_{max} proportionately. Theoretically predicted currents are several times higher than presently observed values.

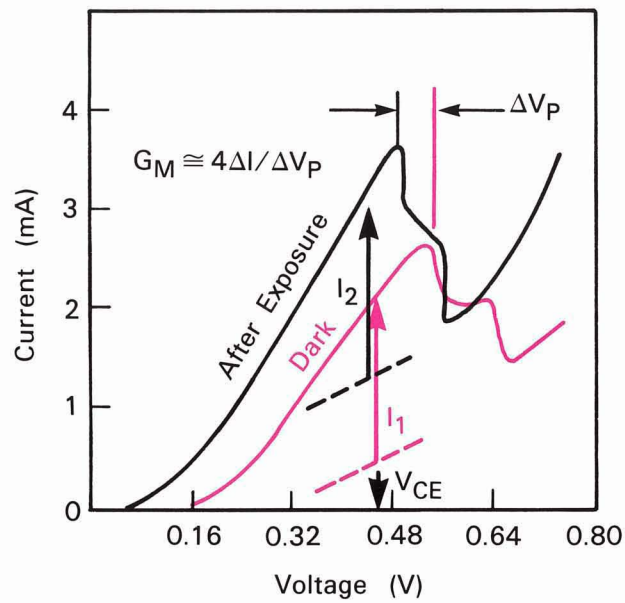

Fig. 13 — These calculated I-V curves for a resonant-tunneling transistor are based upon the assumption that the output impedance of the transistor is large and positive and that the excess current at high voltage can be extrapolated smoothly back to zero.

CONCLUSIONS

Much fertile, yet uncultivated, territory remains in the realm of multiple-barrier tunneling. Three-terminal devices are in their infancy, as are devices for digital applications. The possibility of electro-optical effects has received some attention, and several novel devices have resulted [22]. Most structures to date have contained only two barriers, but investigation of the interaction of three or more barriers may yield even more interesting and useful phenomena.

An extension of multiple-barrier structures to the inclusion of many barriers produces a superlattice. Because of domain formation, superlattices have been impractical electrical devices in the past. Many variations remain untested, even unanalyzed. For example, the "CHIRP" superlattice was examined in some detail [23], but only one type of period variation was investigated. The domain formation that has limited this field to date may be overcome with structures that are yet undeveloped.

All of the devices discussed in this paper have been small compared with their operating

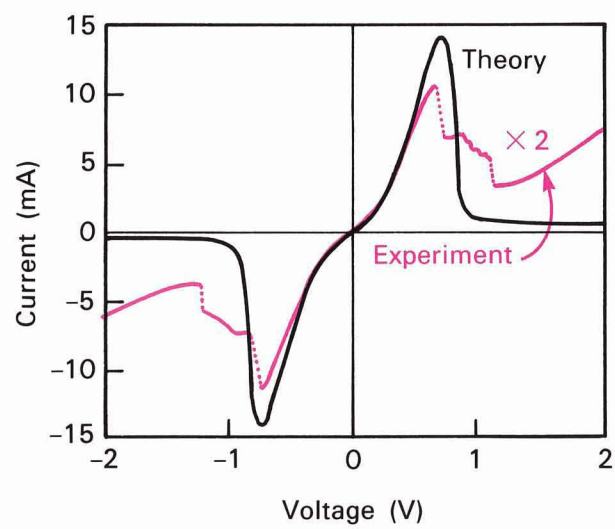

Fig. 14 — The predicted peak-to-valley ratio of a resonant-tunneling device's I-V curve is much greater than that measured for any experimental devices. Improvements in material purity should bring the observed values into closer agreement with the theory.

wavelength. Therefore, they are lumped elements, not transmission media. A bulk material that could provide large, fast impedance nonlinearities would be useful at high frequencies. With two-barrier structures, these nonlinearities are difficult to create, but some variety of superlattice may provide the material necessary for large-scale structures that will find application as traveling-wave devices.

The materials growth that makes possible the high spatial resolution in heterostructure formation is well advanced and progressing rapidly, but much improvement is still possible. Material of sufficient quality for observing reasonable peak-to-valley ratios at room temperature has been available only for two years. Theoretically, as shown in Fig. 14, this peak-to-valley ratio should be much greater. Materials of greater purity could validate most of the assumptions leading to the calculated curve of Fig. 14.

In short, the future of multiple-barrier tunneling structures appears bright, especially in view of the high level of interest in the field. Some of the devices that are just beginning to demonstrate feasibility will be commercially exploited in the next several years and many yet undevised structures will reach the same point in the years to come.

Appendix: Resonant Tunneling Theory

The theory of resonant tunneling is still evolving. The full problem is complicated, involving self-consistent solution of Poisson's equation and the time-dependent Schrödinger equation. The spatial quantization that creates the effects of interest also renders inadequate many of the common approximations used in the solution of these equations. To further complicate matters, scattering from impurities, defects, other carriers, and collective excitations are almost certainly important, but the inclusion of these effects in detail is a difficult theoretical problem. On the positive side, however, the simplest calculations seem to explain the general outline of the experimental observations.

Stationary-State Calculation

The first simplification to make in the analysis of the resonant-tunneling structure is the elimination of time-dependence in the solution of the controlling equations. This stationary-state treatment is based on the approach first applied to finite superlattices by Tsu and Esaki [1]. The calculation shown here incorporates some of our own refinements.

For a first-order solution to the problem, we assume that electrons are the only charge carriers and that they interact only with potential discontinuities in the conduction band. In addition, we use the simplification of the effective-mass model for the electrons. The matching of wave-functions at hetero-interfaces is based on the conservation of probability current, which also accounts for the different effective masses in different semiconductors. We use superposition to determine the potential profile as an electron makes a transit of the structure; the potential is taken as the sum of the potential due to the conduction-band offsets, the applied bias, and any localized charges within the structure. A further, and final, simplifying assumption is that the regions outside the barriers house an electron gas, the field-screening behavior of which is described by the Thomas-Fermi approximation.

The first step in the calculation of a resonant-tunneling I-V curve is the determination of the spatial variation of the electrical potential experienced by the electrons as they transit the double-barrier device under consideration. In addition to the potential change produced by the barrier regions, the electrostatic potential applied by the external (biasing) field produces accumulation and depletion regions that will perturb the potential profile. The spatial dependence of the electrostatic potential, $\phi(x)$, is calculated in the barrier region using the self-consistent Thomas-Fermi equation (cgs units).

$$\phi''(\chi) = \frac{4\pi e n_0}{\epsilon}\left\{1 - \left[1 - \frac{e\phi(\chi)}{E_f}\right]^{3/2}\right\} \qquad \text{(A-1)}$$

where E_f is the Fermi energy, ϵ is the dielectric constant, and n_0 is the average volume-doping density. This expression is solved analytically in the regions with nonzero net charge and then matched numerically at the boundaries. In practice, a parabola is fitted to the solution in the cathode to limit the band-bending region. The spatial extent of the fitted region is taken to be about twice the Thomas-Fermi screening length. A potential profile calculated for a double-barrier structure with doping carrier density of 10^{17} cm^{-3} in the outer regions is shown in the Figure.

Once the potential has been found, the transmission coefficient of an electron with a given energy is determined by using the transfer-matrix method and matching boundary conditions. The current is then found by integrating over the incident electron distribution and the density of available final states [1]. The transfer matrix is numerically calculated for an arbitrary parabolic potential profile. To guarantee rapid convergence, the potential is divided into a few (< 10) spatial segments with transfer matrices calculated for each partition.

Even though the cathode contains an accumulation region, we obtain better agreement between the calculated and measured transmission coefficients if we use the equilibrium Fermi distribution of the cathode material and ignore possible tunneling of the accumulated electrons. This agreement between theory and experiment may be due to the improbability of electrons scattering (inelastically) into the accumulation region, which makes the lifetime for tunneling out of the region shorter than the time for scattering in. However, this means that there is much less band bending than has been assumed.

Temporal Behavior

Time evolution of the system has been eliminated from the stationary-state calculation above. But it is possible to find the lifetime of a transiting electron in the resonant state that it occupies while it is between the two barriers. The approach, first derived for atomic and nuclear resonances, is applicable to any resonant state and can be applied to resonant tunneling. The lifetime is given by the uncertainty relation, $\tau = \hbar/\Delta E$; ΔE is the half-width of the peak in

the transmission coefficient T(E). Frequencies corresponding to $f_{\Delta E} = (2\pi\tau)^{-1}$ are calculated for the three structures and listed in Table 1.

A time-dependent calculation of the electron distribution has been performed by using the Wigner function approach [20]. The time required to reach equilibrium after an impulse to the system is comparable to that estimated by the resonant-state lifetime. This calculation, however, offers the advantage of predicting the time evolution of the wave functions for all times.

Scattering

A complete time-dependent solution should take account of charge redistribution from applied electric fields and motion of carriers through the depletion and accumulation regions. Scattering plays an important part in these processes, because scattering in the barriers removes the assumed condition of conservation of transverse momentum during tunneling, and scattering in the well region or regions destroys the coherence of a carrier wave function over the structure.

According to Luryi [24], scattering may dominate the charge-transport process through a double-barrier structure. His proposal has led to the development of a second, sequential, model of the double-barrier structure. In contrast to the ballistic model, which maintains the coherence of the wave function across the incoming barrier, the sequential model attempts to incorporate the effects of scattering by eliminating the assumption of phase coherence. This model is called the sequential model because each electron is presumed to enter the structure and tunnel through the first barrier, achieve a resonant state within the structure's potential well, and then exit the structure sequentially by tunneling through the remaining barrier. Luryi proposed that all phase coherence is lost before each electron leaves the structure's potential well and that the negative resistance exhibited by the double-barrier device results from the conservation of momentum. When the peak in the density of states in the well (for momentum perpendicular to the well) is below the conduction band edge of the cathode, electrons can not tunnel into the well.

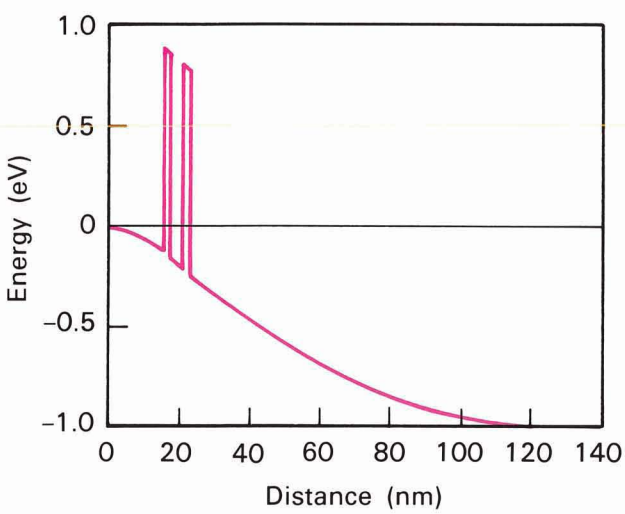

Calculated potential energy of an electron as it transits a double-barrier diode.

Weil and Vinter [25] have recently calculated that the peak current densities should be the same for both the ballistic and the sequential models. It may be, however, that the two models are equivalent as they are presently defined. In their sequential-tunneling calculations, Weil and Vinter use the same boundary conditions as those used for the resonant model (see Ref. 8 in their paper); they maintain the coherence of the wave function across the incoming barrier. The effects of the second barrier enter via the width of the quasibound state in the well, again with a calculation that assumes coherence across the barrier. Perhaps it is not surprising that, with no scattering in the well, the calculations of ballistic and sequential tunneling give the same result.

Weil and Vinter do attempt to include the effects of scattering in the well, via a broadening of the quasibound state. They conclude that, as long as the energy width of this state is small compared to the energy width of the incoming carriers (the usual experimental situation), the lower peak transmission is offset by the additional width. Thus the integral determining the peak current is unaffected. However, the technique of including scattering still implicitly assumes the phase coherence discussed above, even though scattering will generally alter the phase after the scattering event.

This calculation does not appear to be the same as the one originally suggested by Luryi [24] because it does not perturb the phase coherence across the structure. There are also important scattering processes, such as scattering in the barriers, that are not in Luryi's model. Thus the role of scattering remains one of several important unanswered questions in resonant tunneling.

REFERENCES

1. R. Tsu and L. Esaki, "Tunneling in a Finite Superlattice," *Appl. Phys. Lett.* **22,** 562 (1973).
2. L.L. Chang, L. Esaki, and R. Tsu, "Resonant Tunneling in Semiconductor Double Barriers," *Appl. Phys. Lett.* **24,** 593 (1974).
3. T.C.L.G. Sollner, W.D. Goodhue, P.E. Tannenwald, C.D. Parker, and D.D. Peck, "Resonant Tunneling Through Quantum Wells at Frequencies up to 2.5 THz," *Appl. Phys. Lett.* **43,** 588 (1983).
4. M. Tsuchiya and H. Sakaki, "Room Temperature Operation of High-Performance AlAs/GaAs/AlAs Resonant Tunneling Diodes with Atomically Controlled Barrier Width," *IEEE Int. Electron Devices Mtg.*, 662 (1985).
5. T.C.L.G. Sollner, W.D. Goodhue, and H.Q. Le, "Observation of Millimeter-wave Oscillations from Resonant Tunneling Diodes and Some Theoretical Considerations of Ultimate Frequency Limits," *Appl. Phys. Lett.* **50,** 332 (1987).
6. H.R. Fetterman, P.E. Tannenwald, B.J. Clifton, C.D. Parker, W.D. Fitzgerald, and N.R. Erickson, *Appl. Phys. Lett.* **33,** 151 (1978).
7. E.R. Brown, T.C.L.G. Sollner, W.D. Goodhue, and C.D. Parker, "Millimeter-band Oscillations Based on Resonant Tunneling in a Double-barrier Diode at Room Temperature," *Appl. Phys. Lett.* **50,** 83 (1987).
8. C.S. Kim and A. Brandli, "High-frequency High-power Operations of Tunnel Diodes," *IRE Trans. Circuit Theory* **CT8,** 416 (1961).
9. R.F. Trambarulo, *Int. Solid-State Circuits Conf.*, Philadelphia, PA, 1961.
10. P.E. Davis and G. Gibbons, "Design Principles and Construction of Planar Ge Esaki Diodes," *Solid State Electron.* **10,** 461 (1967).
11. D.T. Young, C.A. Burrus, and R.C. Shaw, "High Efficiency Millimeter-Wave Tunnel-Diode Oscillators," *Proc. IEEE* **52,** 1260 (1964).
12. C.A. Burrus, "Gallium Arsenide Esaki Diodes for High-Frequency Applications," *J. Appl. Phys.* **32,** 1031 (1961).
13. E.R. Brown, T.C.L.G. Sollner, and W.D. Goodhue, *Solid State Research Report, MIT Lincoln Laboratory* **1986:1,** 37 (1986).
14. D. Carlson and M.V. Schneider, "Subharmonically Pumped Millimeter-Wave Mixers," *IEEE Trans. Microwave Theory Tech.* **MTT 26,** 706 (1978).
15. C.H. Page, "Harmonic Generation with Ideal Rectifiers," *Proc. IRE* **46,** 1738 (1958).
16. E.R. Brown, T.C.L.G. Sollner, W.D. Goodhue, and C.D. Parker, "Fundamental Oscillations up to 200 GHz in a Resonant-Tunneling Diode," *Device Research Conf.*, Paper IV A 2 (1987).
17. R.J. Nelson, "Long-lifetime Photoconductivity Effect in n-Type GaAlAs," *Appl. Phys. Lett.* **31,** 351 (1977).
18. D.V. Lang, R.A. Logan, and M. Jaros, *Phys. Rev.* B, 1015 (1979).
19. T.C.L.G. Sollner, H.Q. Le, C.A. Correa, and W.D. Goodhue, "Persistent Photoconductivity in Resonant Tunneling Structures: Toward a Resonant Tunneling Transistor," *IEEE/Cornell Conf. Advanced Concepts in High Speed Semiconductor Devices and Circuits*, p. 252.
20. W. Frensley, "Quantum Transport Simulation of the Resonant-Tunneling Diode," *IEEE Int. Electron Devices Mtg.*, Paper 25.5 (1986).
21. A.C. Gossard, "Quantum Well Structures and Superlattices and Their Applications Potential," *Inst. Phys. Conf. Ser.* 69, 1 (1984).
22. F. Capasso, "New Multilayer and Graded Gap Optoelectronic and High Speed Devices by Band Gap Engineering," *Surf. Sci.* **142,** 513 (1984).
23. T. Nakagawa, N.J. Kawai, and K. Ohta, "Design Principles for CHIRP Superlattice Devices," *Superlattices Microstruct.* **1,** 187 (1985).
24. S. Luryi, "Frequency Limit of Double-barrier Resonant-Tunneling Oscillators," *Appl. Phys. Lett.* **47,** 490 (1985).
25. T. Weil and B. Vinter, "Equivalence Between Resonant Tunneling and Sequential Tunneling in Double-barrier Diodes," *Appl. Phys. Lett.* **50,** 1281 (1987).

ACKNOWLEDGMENTS

None of the experimental work described here could have been accomplished without help from staff members skilled in the art of material growth and fabrication. We are especially indebted to W.D. Goodhue for producing excellent quality heterostructures grown by molecular beam epitaxy, for suggesting useful structures, and for overseeing much of the processing. C.L. Chen has also been very helpful in processing, as have G.D. Johnson, K.M. Molvar, W.F. DiNatale, and R.F. Murphy. Expert packaging help has been provided by N. Usiak, D.J. Landers and P.J. Daniels. C.D. Parker has provided considerable expertise with the measurements.

We also owe much to the environment of ideas in which we work. P.E. Tannenwald, B. Lax, C.O. Bozler, A.R. Calawa, B.J. Clifton, M.W. Geis, W.D. Goodhue, M.A. Hollis, R.A. Murphy and H.J. Zeiger at Lincoln Laboratory; F. Capasso and S. Luryi at AT&T Bell Laboratories; W.R. Frensley, R.T. Bate and M.A. Reed at Texas Instruments; M. Heiblum and R.A. Kiehl at IBM; D.D. Coon at the University of Pittsburgh; H. Fetterman at UCLA; H. Sakaki at the University of Tokyo; and L.F. Eastman at Cornell have all contributed to useful technical discussions.

This work was sponsored by the US Army Research Office and by NASA.

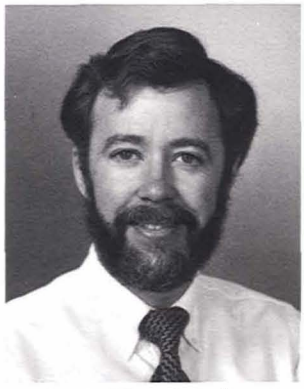

T.C.L. GERHARD SOLLNER is a staff member in the Microelectronics Group. During his five years at Lincoln Laboratory, he has concentrated on novel approaches to high-speed devices. Before coming to Lincoln Laboratory, Gerry was an assistant professor at the University of Massachusetts. He received a bachelor's degree in physics from the Georgia Institute of Technology and a doctorate in physics from the University of Colorado. In his spare time, Gerry enjoys windsurfing, cooking, and skiing.

HAN QUANG LE is a staff member in the Quantum Electronics Group. Before joining Lincoln Laboratory two years ago, he worked for the National Magnet Laboratory at MIT. Han received a PhD in physics from MIT. Han's current research is focused on optoelectronics. In his free time, he enjoys exploring wilderness areas.